applied sciences

MDPI

Article

Structural Performance Optimization and Verification of an Improved Thin-Walled Storage Tank for a Pico-Satellite

Lai Teng * and Zhonghe Jin

School of Aeronautics and Astronautics, Zhejiang University, Hangzhou 310027, China; jinzh@zju.edu.cn
* Correspondence: tenglai@zju.edu.cn; Tel.: +86-571-87952097

Received: 16 October 2017; Accepted: 9 November 2017; Published: 14 November 2017

Abstract: This paper presents an improved mesh storage tank structure obtained using 3D metal printing. The storage tank structure is optimized using a multi-objective uniform design method. Each parameter influencing the storage tank is considered as the optimization factor, and the compression stress (σ), volume utilization ratio (v), and weight (m) are considered as the optimization objectives. Regression equations were established between the optimization factors and targets, the orders of the six factors affecting three target values are analyzed, and the relative deviations between the regression equation and calculation results for σ, v, and m were 9.72%, 4.15%, and 2.94%, respectively. The optimization results showed that the regression equations can predict the structure performance of the improved storage tank, and the values of the influence factors obtained through the optimization are effective. In addition, the compression stress was improved by 24.98%, the volume utilization ratio was increased by 26.86%, and the weight was reduced by 26.83%. The optimized storage tank was developed through 3D metal printing, and the compressive stress was improved by 58.71%, the volume utilization ratio was increased by 24.52%, and the weight was reduced by 11.67%.

Keywords: pico-satellite; propulsion system; multi-objective optimization; storage tank; 3D metal printing

1. Introduction

Storage tanks are widely employed in civil, marine, and automotive fields, etc., to store water, oil, fuel, chemicals, and other fluids. In order to withstand the internal high pressures, a storage tank is generally designed in a cylindrical [1–7], oval [8,9], or spherical [10] shape. This structure and shape affects the performance of the storage tank. A poor design will cause accidental deformation and rupture of the storage tank [3,5]. Thus, the design, optimization, and analysis of storage tanks have received considerable attention from many researchers.

Rastgar and Showkati [11] studied storage tanks at a refinery site by experimentation and finite element analysis (FEA) models. The results show that tanks with oblique body imperfections exhibit high initial strength against buckling due to a uniform external pressure. Azzuni and Guzey [12] investigated a diameter limit for use in the design of the top stiffener ring for above-ground storage tanks using finite-element analysis in a parametric study. The results show that the suitable upper limit to design the top stiffener rings can be increased. Vathi et al. [13] proposed performance criteria for the seismic design of industrial liquid storage tanks and their piping systems, and it can provide a method to introduce industrial components into a performance-based design framework. Sweedan and Damatty [14] developed a simplified design approach to ensure the safety of hydrostatically-loaded combined steel conical tanks against buckling. Numerical examples were presented to explain the application of the suggested design approach. Musa and Damatty [15]

developed a comprehensive design procedure for liquid-filled steel conical tanks under seismic loading. They developed the charts that are used to estimate the capacities of several steel conical tanks, which are then compared to the hydrodynamic loading associated with various seismic zones. Bonanos and Votyakov [16] realized a sensitivity analysis for thermocline thermal storage tank design. They found that the thermocline is sensitive to the tank height, the filler material properties, properties of the fluid, the particle size, void fraction, and a secondary influence from charging times. Erdemir and Altuntop [17] analyzed the thermal stratification of vertically-mounted hot water tanks with four obstacles. They found that placing these obstacles inside the inner tank in vertically-mounted hot water tanks improved the thermal stratification. Ansary et al. [18] developed an optimum design technique for stiffened liquid-filled steel conical tanks subjected to global and local buckling constraints by using a numerical tool that couples a non-linear FEA model developed in-house and a genetic algorithm optimization technique. The optimum design results of these stiffened tanks are verified. Bu and Qian [19] adopted simplified mechanical models to design the top wind girder of large storage tanks. FEA shows that, for a large storage tank with a small height-to-diameter ratio, the strengthening effects of the bottom constraints is significant and should not be ignored. Minoglou et al. [20] developed a simplified, fast, and direct optimum seismic design method, which avoids complicated computational methods like finite element or boundary element methods. The results show that the optimum seismic design is achieved to satisfy the stability of these structures under extreme seismic design loads. Fan and Furbo [21] presented numerical studies of thermal stratification established by standby heat loss from a vertical cylindrical hot water tank. They formed a generalized equation that was implemented in a design program of an existing tank optimization in order to estimate its thermal performance. Niloufari et al. [22] studied the buckling behavior of thin-walled tank shells via tests. This study shows that geometrical imperfections at different ratios of t/R may have decreasing, neutral, or increasing effects on buckling resistance and can result in a softening or stiffening behavior of the shells.

These studies are mainly used at ground level for relatively large storage tanks. Aerospace storage tanks, especially satellite propulsion storage tanks, require much more stringent requirements for their performance. A propulsion system has a direct impact on the life, reliability, orbit, and altitude control of a pico-satellite. Hence, it is an important component of pico-satellites [23]. With the continuous development of pico-satellites, the design of each system encountered by the satellite has many new challenges. The installation space constraints are the most obvious. Experts and scholars studying propulsion systems are concerned about the problems of improving the structure strength, the ability of the system to carry propellant, and the propulsion efficiency in a limited space.

A micro-satellite propulsion system is limited by the performance, installation space, and weight. Chemical propulsion, electric propulsion, and laser propulsion systems have further limitations, such as a complex structure, a large volume, and a large weight [24–26]. Hence, they cannot be applied to micro-satellites. A pico-satellite or nano-satellite has a smaller volume and weight. Therefore, the installation and volume utilization rate of the propulsion system becomes more of a prominent problem. Currently, a pico-satellite mainly uses a storage tank propulsion system that is a high-pressure, thin-walled storage tank [27,28]. Owing to the requirements of the processing method, pressure, and weight, conventional propulsion storage tanks are oval or spherical in shape. When the storage tank occupies the same installation envelope, the volume utilization rate is low. To fully utilize the installation space for a pico-satellite, the conventional storage tank must be changed to a complex or special-shaped storage tank. A rational design can effectively improve the strength and volume utilization rate, and can reduce the weight [29,30].

With the rapid development of 3D metal printing technology, its scope of applications has gradually broadened while its performance has continuously improved. This technique is widely used in the aerospace, automotive, and medical fields [31–33]. This kind of manufacturing method without conventional tools or molds can realize complex structures that are difficult to process using conventional processes. It can simplify the production process, shorten the manufacturing cycle, and reduce cost. With the use of high-strength materials, such as titanium alloy, aluminum alloy, and

nickel alloy, in printing [34,35], the mechanical properties and appearance are comparable to those obtained from conventional machining methods. A conventional storage tank only withstands pressure through the internal wall, but when using 3D metal printing, it can be designed as a mesh structure, which can withstand higher pressure, improve the volume, and reduce the weight. Even the pipelines and other storage tank accessories can be printed directly. This new process method facilitates the development of an improved storage structure for propulsion systems [36–38].

This paper presents an improved mesh storage tank structure obtained using selective laser melting (SLM) 3D metal printing. The storage tank is optimized using a multi-objective uniform design method. The parameters of the mesh structure, such as the length, three direction intervals, wall thickness, and the connecting distance to the side wall, are considered the optimization factors. The compressive stress, volume utilization ratio, and weight parameters are considered the optimization objectives. Optimization factors and targets for the storage tank are shown in Table 1. Regression equations are established between the optimization factors and targets, the orders of the six factors affecting the three target values are analyzed, and the validity of the regression equation is verified. The values of the influence factors are obtained via optimization. The relative deviations between the regression equation and calculation results are analyzed, and the improvements for compressive stress, volume utilization ratio, and weight are discussed. The optimization results are verified via experiments; consequently, the compressive stress is improved, the utilization rate is increased, and the weight is reduced.

Table 1. Optimization factors and targets for the storage tank.

Optimization Factors	Optimization Targets
Length (d)	Compression stress (σ)
Three direction intervals (d_x , d_y , and d_z)	volume utilization ratio (v)
Wall thickness (T)	Weight (m)
Connecting distance to the side wall (D)	

2. Propulsion System Structure

2.1. Conventional Storage Tank Structure

A propulsion system consists of a storage tank, pipeline, filter, pressure sensor, filling port, isolation valve, electromagnetic valve, thruster, etc., is shown in Figure 1. The propulsion system uses liquid ammonia as the propellant and relies on ammonia under pressure at the ordinary temperature for liquefaction. The control commands causes the thruster to open and close as ammonia is sprayed from the thruster under the action of saturated ammonia vapor. In a vacuum environment, owing to the flash evaporation characteristics of liquid ammonia, a rapid evaporation of ammonia occurs in the nozzle. Ultimately, liquid ammonia becomes a two-phase flow state to be sprayed and can generate thrust to provide the impulse for satellite orbit control.

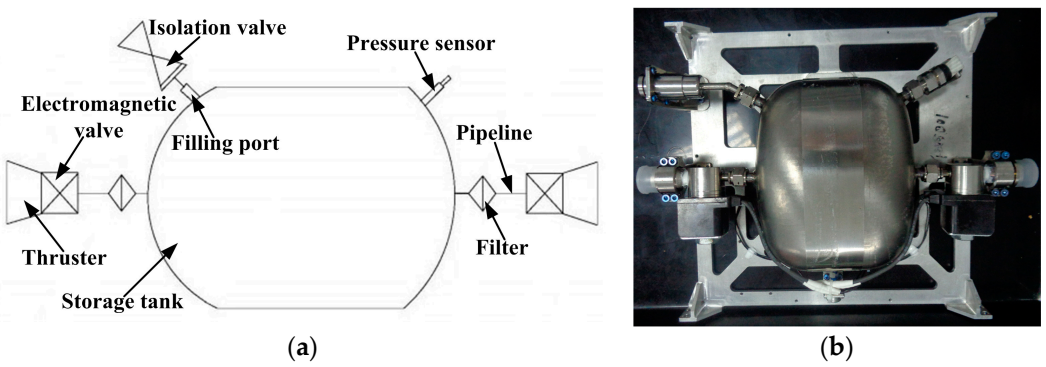

Figure 1. Propulsion system composition (**a**) design diagram; and (**b**) the actual propulsion system.

Owing to the limitation of the envelope size, the storage tank is designed to be an approximate cylindrical structure with an oval cross-section. Its shape and overall structure are shown in Figure 2. The storage tank is made of Ti-6Al-4V or TC4 (annealed), and the overall parameters of the tank are as follows: height of 66 mm, width of 130 mm, length of 112 mm, thickness of 2.1 mm, mass of 0.368 kg, and volume of 0.607 L.

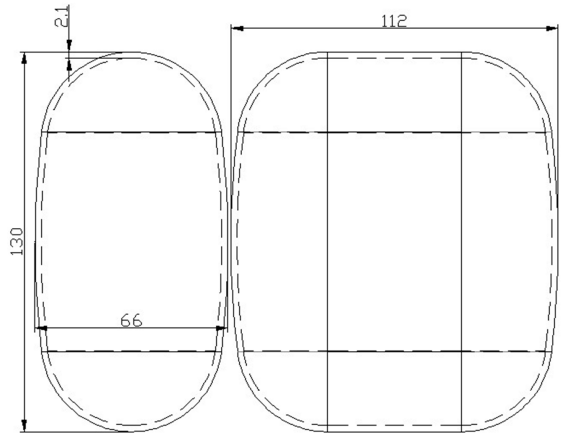

Figure 2. Shape and dimension of the conventional storage tank.

Since the installation space inside a pico-satellite is limited, the envelope occupied by the storage tank is fixed, and a conventional oval and spherically-shaped storage tank will result in a significant space loss for the same envelope. The volume utilization rate of elliptical and spherical shapes is approximately 60%. Among all of the shapes, a cuboid has the largest envelope. In order to guarantee the installation and enhance the structural performance of a storage tank in an envelope of limited space, the structure of the storage tank must be improved.

2.2. Improved Storage Tank Structure

In order to withstand the greater pressure load and for ease of manufacturing, conventional storage tanks in a pico-satellite have a hollow structure inside and require a high wall thickness. Moreover, a fixed storage tank requires additional accessories which reduces its volume utilization rate and increases the overall weight. In addition, in traditional processing methods, such as electrode welding, the processing cycle is long, or unable to fully complete, and the cost is very high. In order to solve these problems, this paper presents an improved mesh storage tank structure obtained using 3D metal printing by changing the shape of the conventional storage tank. When the overall size of the envelope is fixed, increasing the internal reinforcement structure and reducing the wall thickness to use the volume of a conventional storage tank is impractical. A solution requires an improved compressive stress, increased volume utilization rate, and reduced weight.

The internal structure utilizes a mesh structure in order to further optimization. This is a single column structure with a square or circular cross shape. When the envelope of the storage tank uses the shape shown in Figure 2, the structure of the storage tank is determined by the length d of the mesh structure, three direction intervals d_x, d_y, and d_z, wall thickness T, and the connecting distance to the side wall D, as shown in Figure 3.

In order to ensure an equal length design of the storage tank in all the three directions, a cylindrical structure with the same length is adopted into the three directions, and the connection distance to the side wall is equal. According to the characteristics of the mesh structure, the distance to the wall, which is equal in the three directions, can be expressed as:

$$d_i = (i - 2d - 2D)/(n_i - 1) \qquad i = x, y, z \tag{1}$$

where, x, y, z represent the envelope size of the tank in three directions, respectively, and n_i represents the number of columnar structures in three directions.

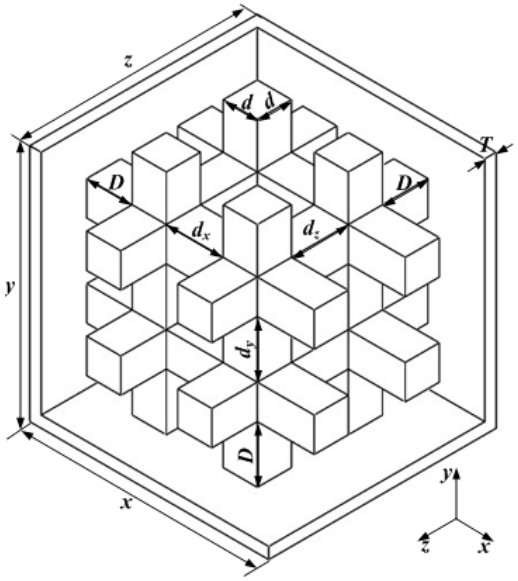

Figure 3. Diagram of the structural parameters of the modified storage tank.

3. Storage Tank Performance Analysis

3.1. Mechanical Property Measurements

To obtain the properties of the 3D printing material, three tensile specimens are pre-printed. The size of the pre-printed tensile specimens are as follows: length of 80 mm and diameters of 20 mm and 15 mm. The related introduction for additive manufacturing and post-processing steps for pre-printed tensile specimens are show in Table 2 and Figure 4. The dimensions of tensile specimens are selected based on the recommended dimensions of the Instron 3382 tensile testing machine (Instron, Boston, MA, USA). In Figure 5, the print direction, 3D printing specimens, tensile specimen size, tensile test, and true stress–strain [39] diagram of the material are shown. The final mechanical properties of the specimens are given in Table 3.

Table 2. Related introduction for additive manufacturing.

Content	Parameter
Material	Ti-6Al-4V (Annealed)
Powder size	15–53 μm
SLM equipment	BLT-S310
Temperature	2200–2800 °C
Layer height	0.06 mm
Laser type	500 W Fiber Laser
Heat treatment	800 °C , Holding time 2 h

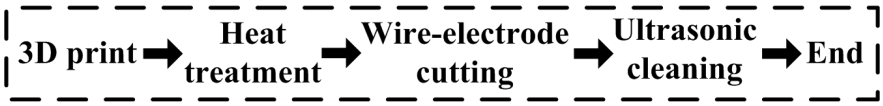

Figure 4. Post processing steps for pre-printed tensile specimens.

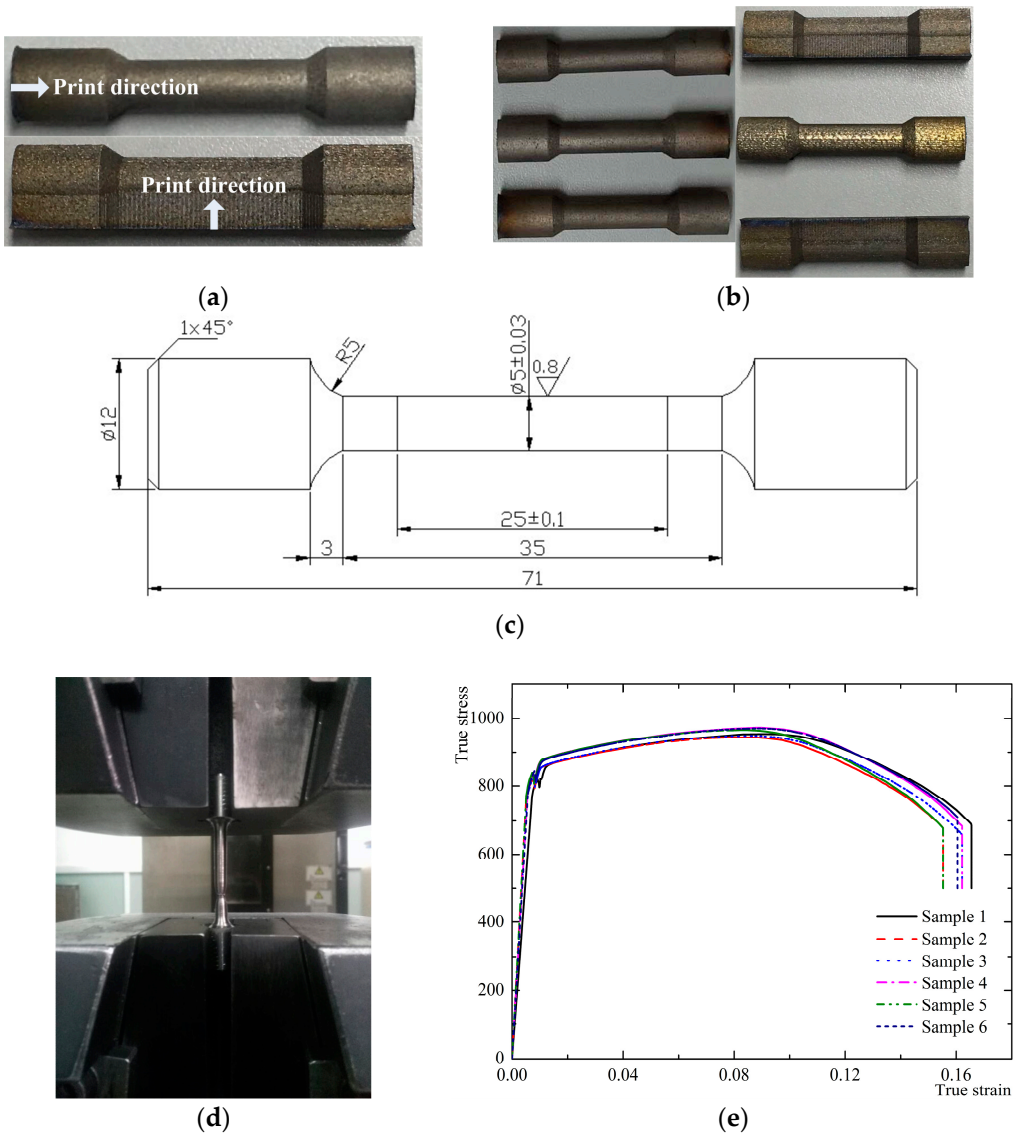

Figure 5. (**a**) The print direction; (**b**) 3D printing specimens; (**c**) tensile specimens size; (**d**) tensile test; and (**e**) true stress-strain of material.

Table 3. Material properties.

Material	Density/kg/m³	Young's Modulus/GPa	Poisson Ratio	Yield Strength /MPa	Tensile Strength/MPa
Ti-6Al-4V	4500 [40]	113.8	0.31	820.8	959.1

3.2. Compressive Stress Analysis

The performance of the storage tank is mainly evaluated in terms of the compressive stress, volume utilization rate, and weight. We utilize conventional, rectangular, and improved tank structures whose envelope dimensions are: length, 112 mm; width, 130 mm; and height, 66 mm. Furthermore, a single column structure with a square or circular cross shape is used. We suppose that the length and diameter of the single column structures are both 1.5 mm, and the number of the single column structures in three directions are assumed to be 9, 17, and 19, respectively. The wall thickness is assumed to be 0.5 mm, and the connecting distance to the side wall is 5.5 mm. The wall thickness of the conventional and cuboid storage tanks are 2.1 mm and 0.5 mm.

The propulsion system is also used for the storage of the liquid ammonia container. This choice mainly helps the system withstand the internal pressure load. A system that can withstand a higher pressure of saturated ammonia steam, which can provide greater thrust to the propulsion system leading to a more stable performance.

We used Solidworks design software (Dassault Systemes S.A, Concord, MA, USA, 2014) to build six kinds of 1/8 storage tank models to analyze the compressive stress. The size of each storage tank model mesh is 8 mm. In order to improve the calculation efficiency we used a large mesh size. Though the mesh size is very large, it can acquire the rough stress values of different storage tanks while not affecting the trend analysis of the stress. The boundary conditions in the three directions are the symmetry constraints and the 2.4 MPa pressure applied to the inner wall. We input the density, Young's modulus, Poisson ratio, yield strength, and tensile strength into ABAQUS finite element software (Dassault Systemes S.A, Concord, MA, USA, 2013), which we used to directly perform static ideal elastic-plastic modelling.

The analysis results of the strength of the storage tank are shown in Figure 6. The stresses of the four kinds of storage tanks used are 417 MPa, 1357 MPa, 1488 MPa, 2737 MPa, 214 MPa, and 122 MPa, respectively. The results show that the thinner walled storage tank can reduce mass, but it can be subject to greater stress, buckling, and rupture, as shown in Figure 6c,d. The improved mesh structure with the square column structure can withstand a greater pressure load. Hence, we abandon the schemes of Figure 6c,d.

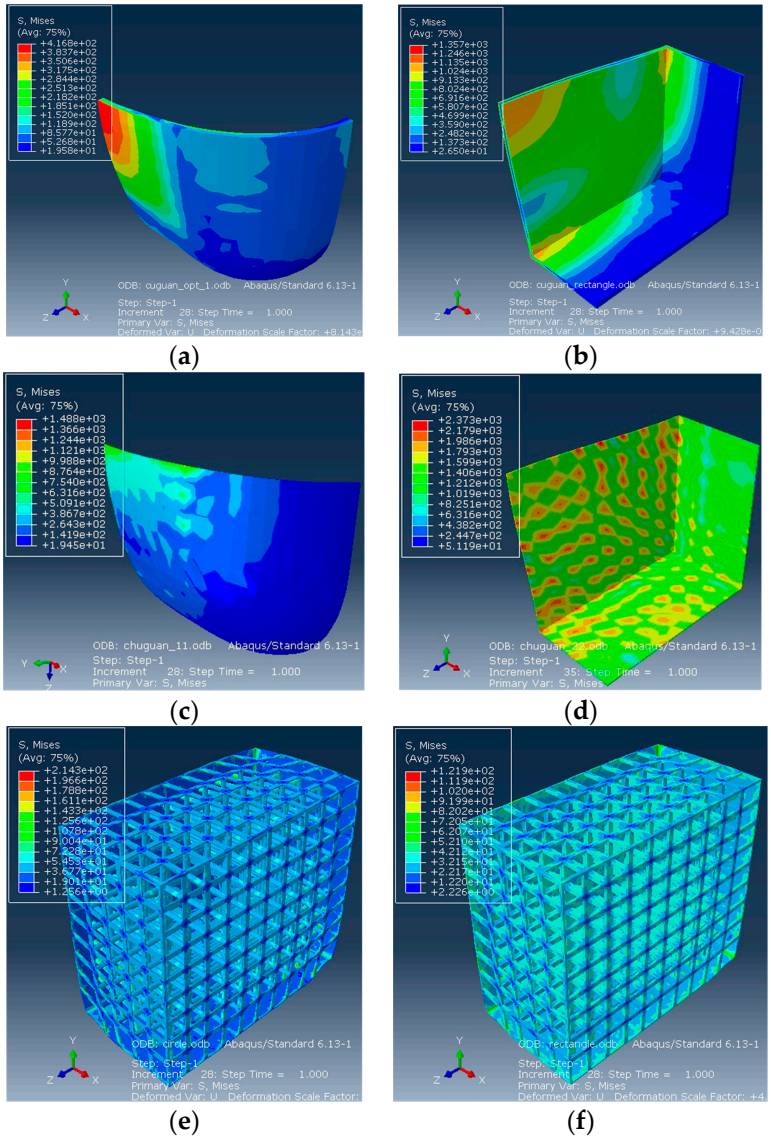

Figure 6. Stress analysis figure for (**a**) the conventional storage tank (wall thickness: 2.1 mm), (**b**) the cuboid storage tank (wall thickness: 2.1 mm), (**c**) the conventional storage tank (wall thickness: 0.5 mm), (**d**) the cuboid storage tank (wall thickness: 0.5 mm), (**e**) the improved storage tank with a circular column structure, and (**f**) the improved storage tank with a square column structure.

3.3. Volume Utilization Rate Analysis

The higher the volume utilization ratio of the tank, the more propellant it can carry. It can prolong the life of the propulsion system and improve the control capability of the altitude and orbit of the satellite [41]. The volume utilization rate refers to the ratio of volume of the inner liquid to the volume of the envelope. The volume utilization ratios of the four storage tanks are denoted as v_C, v_R, v_r, and v_S, and they can be expressed as:

$$v_C = \iint_{D_1} f_C \mathrm{d}x\mathrm{d}y / xyz \tag{2}$$

$$v_R = (x-2T)(y-2T)(z-2T) / xyz \tag{3}$$

$$v_r = \left\{ (x-2T)(y-2T)(z-2T) - d^2 \left[(x-2T)n_y n_z + (y-2T)n_x n_z + (z-2T)n_x n_y \right] - 2n_x n_y n_z \iint_{D_2} f_r \mathrm{d}x\mathrm{d}y \right\} / xyz \tag{4}$$

$$v_S = \left\{ (x-2T)(y-2T)(z-2T) - d^2 \left[(x-2T)n_y n_z + (y-2T)n_x n_z + (z-2T)n_x n_y - 2dn_x n_y n_z \right] \right\} / xyz \tag{5}$$

where v_C is the volume utilization ratio of the conventional storage tank, v_R is the volume utilization ratio of the cuboid storage tank, v_r is the volume utilization ratio of the improved storage tank with a circular column structure, and v_S is the volume utilization ratio of the improved storage tank with a square column structure. f_C is the functional expression when the propellant forms an enclosed area D_1 in the conventional storage tank. f_r is the functional expression when three cylindrical structures form a closed area D_2 at the intersection.

The calculation results of the propellant volume and volume utilization rates of the four kinds of storage tanks are presented in Table 4. The propellant volume and volume utilization rate of the conventional storage tank are lower than those of other types of tanks; however, there is considerable room for improvement of the conventional storage tank for carrying the propellant.

Table 4. Propellant volume and volume utilization ratio of four storage tanks.

Name	Conventional	Rectangular	Improved (Circular)	Improved (Square)
Propellant volume/ dm^3	0.607	0.838	0.839	0.816
volume utilization rate	63.22%	87.2%	87.32%	84.95%

3.4. Weight Analysis

Weight reduction directly determines the performance of the product and launch cost [42,43] and, hence, is a major concern in the aerospace field. If the weight of the storage tank is greater for the same envelope and the effective volume occupied by the storage tank is greater, it can carry less propellant. Therefore, we must consider trade-offs when improving the strength and volume utilization rate of storage tanks.

Depending on the volume of propellant to be filled in the storage tank, the mass of the cuboid, improved storage tanks with a circular and square column structure can be expressed as:

$$m_i = \rho(1 - v_i)xyz \tag{6}$$

The weights of the four storage tanks are listed in Table 5. The results show that the conventional storage tank has a significant advantage in weight, and the improved storage tank needs to be optimized in terms of weight reduction.

Table 5. Weight of four storage tanks.

Conventional	Rectangular	Improved (Circular)	Improved (Square)
368	553	549	652

4. Structural Performance Optimization of Storage Tank

According to the comparison of the three structural performances in the previous section, i.e., compressive stress, volume utilization rate, and weight, the structural performance of the conventional storage tank would be significantly improved by changing its structure. As the conventional tank is oval, the corresponding reinforcement and accessories must be increased for installation in a satellite and, hence, the weight of the conventional storage tank is increased to 600 g. The improved storage structure with square column structure can be directly installed, and the installation can reduce the weight and simplify the installation process. Through the analysis of the compressive stress, volume utilization rate, and weight of conventional storage tanks, the optimization objectives for the structural performance of improved storage tanks are determined, as presented in Table 6. Structural performance optimization of a storage tank, the optimization equations, different variables, and constraints can be expressed as:

$$\text{Minimize} \begin{cases} \sigma(d, n_x, n_y, n_z, T, D) = \sigma - 400 \\ v(d, n_x, n_y, n_z, T, D) = v - 96 \\ m(d, n_x, n_y, n_z, T, D) = m - 400 \end{cases} \quad (7)$$

$$\text{Subject to } 0.5 \le d \le 1.5,\ 11 \le n_x, n_y, n_z \le 21,\ 0.3 \le T \le 0.8,\ 2 \le D \le 7.$$

Table 6. Optimization target of structural performance of the improved storage tank with a square column structure.

Structural Performance	Before Optimization	After Optimization
σ (Compression stress)	416 MPa	≤400 MPa
v (Volume utilization ratio)	63.22%	≥94%
m (Weight)	600 g	≤400 g

4.1. Optimization Method of Structural Performance

Generally, in a multi-factor test, increased numbers of factors and levels cause an exponential increase in the number of tests to be conducted. The determinant factors for the structural performance of a storage tank are length d, mesh structure numbers in the three directions n_x, n_y, and n_z, wall thickness T, and connecting distance to the side wall D. According to the characteristics of these factors, we can adopt a parametric test method. Twenty-five tests are required for six factors and four levels, whereas for six factors and six levels, 49 tests are required. However, for six factors and 11 levels, orthogonal tests cannot be created. A uniform design can solve the multi-factor and multi-level problems, and this requires fewer test combinations to obtain the influence of each factor on the target value, or even determine the value of each factor when it arrives at a satisfactory target value.

4.2. Optimization Process of Structural Performance Parameters

According to the analysis results in Section 3, the improved storage tank with a square column structure has less compressive stress, a greater volume utilization rate, a lighter weight, and more room for improvement; therefore, we select and optimize the improved storage tank with the square column structure. Owing to the precision limit of 3D metal printing, the precision fluctuation is in the range of −0.3–0.3 mm during the process of printing. When the accuracy is limited, the fluctuation can become 0–0.2 mm. In order to prevent the optimized parameters from not printing as well as convenient optimization, we select d in the range of 0.5–1.5 mm, n_x, n_y, and n_z in the range of 11–21, T in the range of 0.3–0.8 mm, and D in the range of 2–7 mm.

According to the ranges of factors affecting the performance of the storage tank structure, the parameter level table is established, as presented in Table 7. Without considering the interaction

among various factors, the parameter level table of six factors and 11 levels is established. Eleven types of storage tank models are built and inputted into ABAQUS FEA software. The parameter level table, calculation, and simulation results are listed in Table 8.

Table 7. Parameter-level table for the improved storage structure with a square column structure.

No.	d	n_x	n_y	n_z	T	D
1	0.5	11	11	11	0.3	2
2	0.6	12	12	12	0.35	2.5
3	0.7	13	13	13	0.4	3
4	0.8	14	14	14	0.45	3.5
5	0.9	15	15	15	0.5	4
6	1.0	16	16	16	0.55	4.5
7	1.1	17	17	17	0.6	5
8	1.2	18	18	18	0.65	5.5
9	1.3	19	19	19	0.7	6
10	1.4	20	20	20	0.75	6.5
11	1.5	21	21	21	0.8	7

Table 8. Uniform test table and the calculation and finite element analysis results for the improved storage structure with a square column structure.

No.	d	n_x	n_y	n_z	T	D	σ	v	m
1	2	8	8	4	4	11	1142	96.974	259
2	9	10	5	1	3	5	998.9	88.498	620
3	6	9	2	10	9	9	286.7	91.911	552
4	1	2	6	11	5	4	1251	98.165	224
5	7	3	9	3	8	2	340.6	92.519	511
6	5	6	1	6	1	1	1169	95.134	299
7	3	5	4	2	11	7	992.4	97.241	343
8	4	11	11	7	7	6	544.5	92.841	483
9	10	1	3	5	6	10	167.5	91.152	544
10	11	7	7	8	10	3	105	82.421	985
11	8	4	10	9	2	8	295.3	88.333	614

Most of the experimental design methods usually use the variance and regression analysis to process the data. The test of the uniform design is relatively small. In order to not realize the analysis of variance, the regression analysis is the main method of uniform design. If the factor level is greater than the number of test factors, two regression analyses can be used. This paper can only use multiple linear regression analysis, so the σ, v, and m of the linear regression equations can be expressed as:

$$\sigma = 3495.159 - 1052.56d + 11.322n_x - 32.522n_y - 41.299n_z - 986.523T - 52.676D \quad (8)$$

$$v = 120.027 - 13.227d - 0.335n_x - 0.272n_y - 0.302n_z - 1.719T + 0.219D \quad (9)$$

$$m = -882.686 + 583.4421d + 14.679n_x + 12.058n_y + 13.549n_z + 350.334T - 9.784D \quad (10)$$

We want to know which factors influence the target values significantly. In order to determine the influence of each factor on the target value, we must analyze the statistic of the regression coefficient, that is, p value analysis. When the p value is lower than the significance level 0.05, indicating that the factors are related to the target value, a lower p value indicates a stronger effect on the target value. The analysis results are shown in Table 9.

From Table 9, we can obtain the effect of the p values of six factors on σ, v, and m. The orders of the six factors affecting σ, v, and m are $d > T > n_z > n_y > D > n_x$, $d > n_x > n_z > n_y > D > T$ and $d > T > n_x > n_z > n_y > D$, respectively. This shows that d most strongly affects σ, v, and m, and d is related to the three target values, having the strongest dependency between d and v. Moreover, T also affects m, and T is related to m. Other factors have weaker effects and dependencies on these three target values.

Table 9. The analysis results of p value for σ, v, and m.

Factor	p Value for σ	p Value for v	p Value for m
Length (d)	0.011	6.359×10^{-4}	6.512×10^{-4}
Structure numbers in x direction (n_x)	0.656	0.071	0.073
Structure numbers in y direction (n_y)	0.236	0.116	0.117
Structure numbers in z direction (n_z)	0.154	0.092	0.089
Wall thickness (T)	0.1	0.559	0.043
Connecting distance to the side wall (D)	0.321	0.465	0.462

We use 1stOpt software to optimize σ, v, and m, where the detailed optimization settings are shown in Table 10. When σ, v, and m are set to the target values, we can obtain the values of each parameter. According to the orders of the six factors affecting σ, v, and m, and in order to facilitate the processing, modelling, and calculation for the final printing, the final value of each parameter is selected to be equal or greater than the optimal value of each parameter. The optimal values are listed in Table 11. The optimization process, optimization results, and calculation results are shown in Figures 7–9, respectively.

Table 10. The optimization settings.

Optimization Algorithm	Levenberg-Marquardt
Convergence judgment index	1×10^{-10}
Maximal iterated algebra	10,000
Real time output control number	5000
Times	200
Control iteration algebra	300
Convergent judgment algebra	15

Table 11. Optimization and final value of storage tank structure parameters.

Optimization Factor	Optimization Value	Final Value
Length (d)	0.916 mm	1 mm
Structure numbers in x direction (n_x)	11.000	11
Structure numbers in y direction (n_y)	16.875	17
Structure numbers in z direction (n_z)	20.976	21
Wall thickness (T)	0.478 mm	0.5 mm
Connecting distance to the side wall (D)	6.999 mm	7 mm

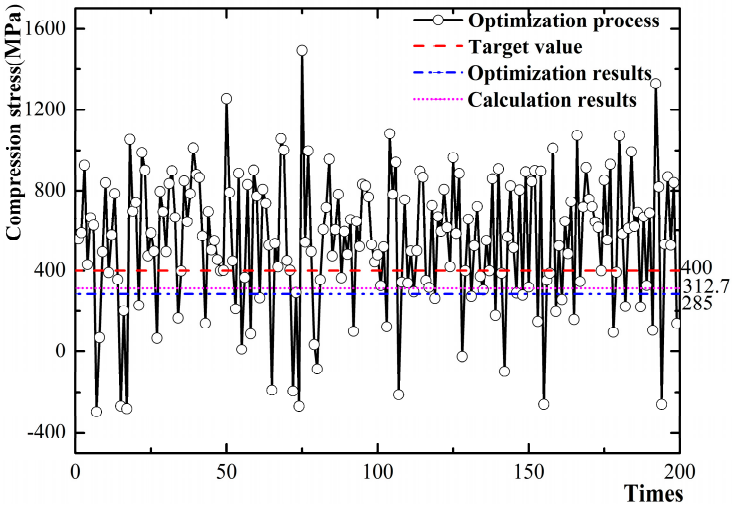

Figure 7. Compression stress optimization process, optimization results, and calculation results.

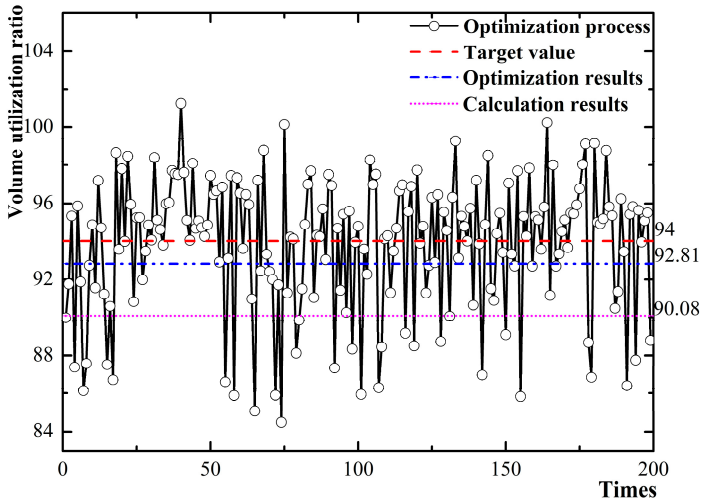

Figure 8. Volume utilization ratio optimization process, optimization results, and calculation results.

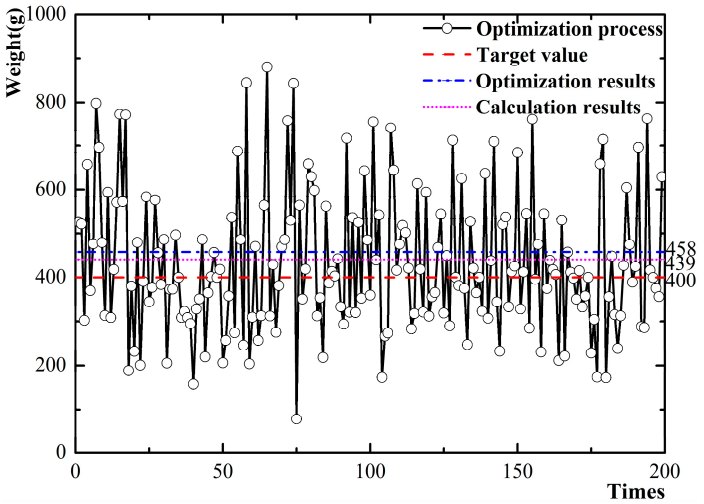

Figure 9. Weight optimization process, optimization results, and calculation results.

According to the analysis results, the relative deviations of compressive stress, volume utilization rate, and weight between the optimization results and calculated results are 9.72%, 2.94%, and 4.15%, respectively. It has been demonstrated that the established regression equation can predict the structural performance of the improved storage tank.

5. Simulation Analysis and Test Verification

According to the results of the parameter optimization, we established a storage tank model. According to Equations (5) and (6), we calculated the volume utilization rate and the weight of the improved storage tanks as 90.08% and 439 g, respectively. We obtained the compressive stress as 312.7 MPa via simulation analysis. In order to prevent a stress concentration between the columnar structure and connecting surface by 3D printing, we increased the fillet at the connecting surface position and, hence, the corresponding performance will change after it loads the same pressure. The compressive stress was 172.1 MPa and the results are shown in Figure 10.

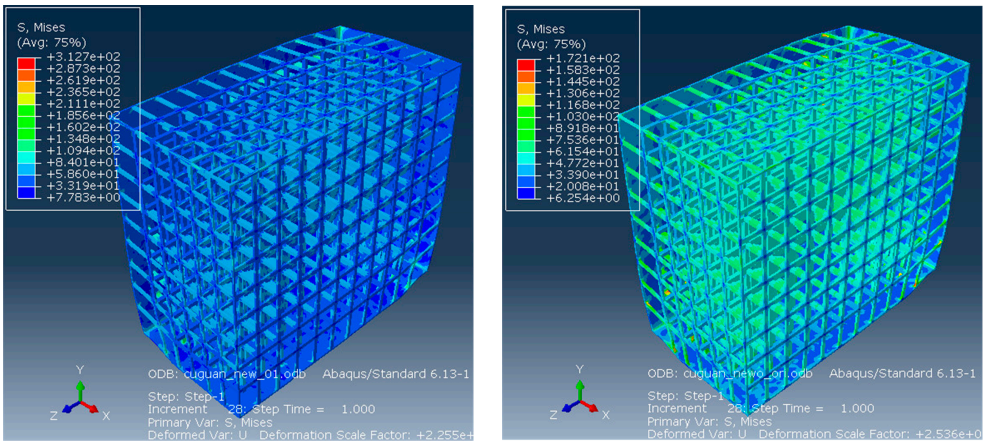

(**a**) (**b**)

Figure 10. Stress analysis figure for (**a**) the improved storage tank after optimization; and (**b**) the improved storage tank after post-processing.

The 3D metal printing of the improved storage tank structure is based on the optimization results in Table 11. The print direction of the storage tank, post-processing steps for the storage tank, and the optimized structure of the storage tank was manufactured via a 3D metal printing process as shown in Figures 11–13. The structural performance is compared before and after optimizing the storage tank. The comparison of the storage tank structural performance before and after optimization is presented in Table 12. It can be determined from Table 12 that the compressive stress was improved by 24.98%, the volume utilization ratio was increased by 26.86%, and the weight was reduced by 26.83%. The optimized storage tank was developed via 3D metal printing. Owing to the error of processing, the improved storage tank of the trial manufacture increases the weight, whereas our storage tank weight was reduced by 11.67%. According to Equation (6), the volume utilization ratio can be increased by 24.52%. According to the calculation, the compressive stress can be increased by more than 58.71%.

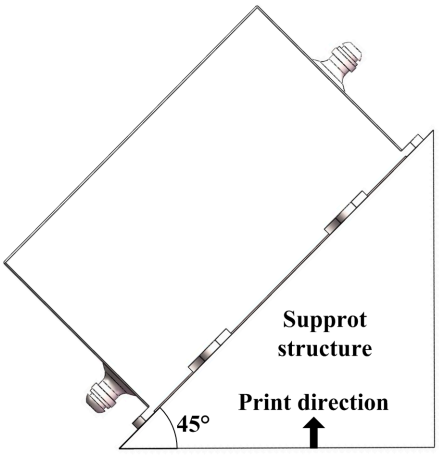

Figure 11. The print direction of the storage tank.

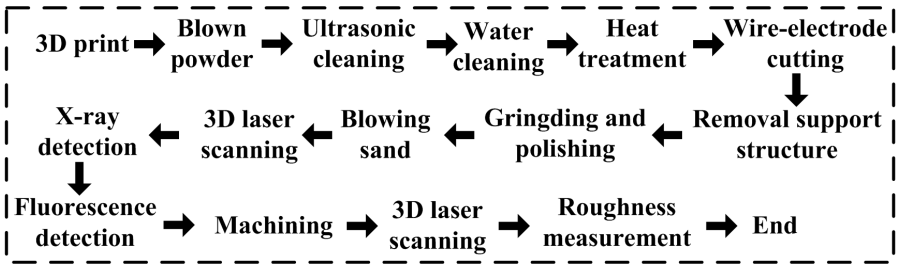

Figure 12. Post-processing steps for storage tank.

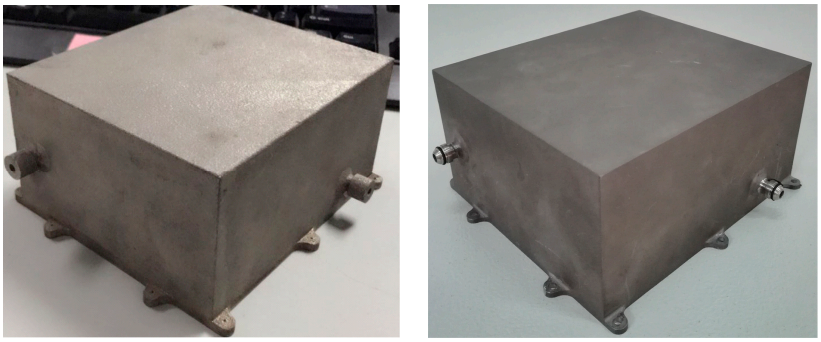

(**a**) (**b**)

Figure 13. 3D metal print storage tank (**a**) before optimization; and (**b**) after post-processing.

Table 12. Comparison of structural performance of storage tank before and after optimization.

Structural Performance	Conventional Storage Tank	Improved (Square) Storage Tank	Improved (Square) Storage Tank after Post Processing	3D Printing Storage Tank after Post Processing
σ (Compression stress)	416.8	312.7	172.1	<172.1
v (Volume utilization ratio)	63.22%	90.08%	90.03%	87.74%
m (Weight)	600	439	441	530

6. Discussion

The price of SLM equipment is higher than traditional equipment and forming powder has a higher price than traditional raw materials. Therefore, SLM is not suitable for processing general parts, the size range for forming parts is limited, and it cannot process large-sized parts. Spheroidizing and warpage are major defects in the SLM forming process. The SLM method can be used to obtain arbitrarily-sized shapes and fully-metallurgical functional parts. The density can reach 100%, a size precision of 20–50 μm, and a surface roughness of 20–30 μm. It can greatly shorten the manufacturing cycle, and its application scope has been extended to the fields of aerospace, medicine, automotion, molds, etc.

7. Conclusions

(1) This paper presents an improved mesh storage tank structure obtained using 3D metal printing by changing the shape of the conventional storage tank. When the overall size of the envelope is fixed, increasing the internal reinforcement structure and reducing the wall thickness can use the volume of a conventional storage tank that cannot otherwise be utilized, and improve the compressive stress, increase the volume utilization rate, and reduce the weight.

(2) The storage tank is optimized using a multi-objective uniform design method. Regression equations are established between the optimization factors and targets, the orders of the six

factors affecting the three target values are analyzed, and the validity of the regression equation is verified. The values of the influence factors are obtained via optimization.

(3) The optimization results are verified via simulation and experiments. The compression stress is improved by 24.98%, the volume utilization ratio is increased by 26.86%, and the weight was reduced by 26.83%. The optimized storage tank was developed through 3D metal printing, and the compressive stress is improved by 58.71%, the volume utilization ratio is increased by 24.52%, and the weight is reduced by 11.67%.

Acknowledgments: The authors thank Xi'an Bright Laser Technologies Co. Ltd. provided selective laser melting (SLM) for the support extended towards this research work.

Author Contributions: Lai Teng have made substantial contributions to design of the work, designed experiment, collected data and and implemented analysis, drafted the work. Final approval of the version to be published. Agreement to be accountable for all aspects of the work in ensuring that questions related to the accuracy or integrity of any part of the work are appropriately investigated and resolved. Zhonghe Jin have made substantial contributions to the conception of the work, and revised it critically for important intellectual content. Final approval of the version to be published. Agreement to be accountable for all aspects of the work in ensuring that questions related to the accuracy or integrity of any part of the work are appropriately investigated and resolved.

Conflicts of Interest: The authors declare no conflict of interest.

References

1. Bouhal, T.; Fertahi, S.; Agrouaz, Y.; Rhafiki, T.E.; Kousksou, T.; Jamil, A. Numerical modeling and optimization of thermal stratification in solar hot water storage tanks for domestic applications: CFD study. *Sol. Energy* **2017**, *157*, 441–455.
2. Shamsi, H.; Boroushaki, M.; Geraei, H. Performance evaluation and optimization of encapsulated cascade PCM thermal storage. *J. Energy Storage* **2017**, *11*, 64–75.
3. Godoy, L.A. Buckling of vertical oil storage steel tanks: Review of static buckling studies. *Thin-Walled Struct.* **2016**, *103*, 1–21.
4. Zheng, Y.H.; Li, Y. Research on the Vibration Characteristics of Vertical Cylindrical Shell Container. *J. Xihua Univ.* **2016**, *35*, 24–28.
5. Godoy, L.A.; Batista-Abreu, J.C. Buckling of fixed-roof aboveground oil storage tanks under heat induced by an external fire. *Thin-Walled Struct.* **2012**, *52*, 90–101.
6. Manshadi, S.H.D.; Maheri, M.R. The effects of long-term corrosion on the dynamic characteristics of ground based cylindrical liquid storage tanks. *Thin-Walled Struct.* **2010**, *48*, 888–896.
7. Firouz-Abadi, R.D.; Haddadpour, H.; Kouchakzadeh, M.A. Free vibrations of composite tanks partially filled with fluid. *Thin-Walled Struct.* **2009**, *47*, 1567–1574.
8. Liu, Y.W.; Liu, X.; Yuan, X.Z.; Wang, X.J. Optimizing design of a new zero boil off cryogenic storage tank in microgravity. *Appl. Energy* **2016**, *162*, 16778–1686.
9. Yuan, X.Z.; Wang, X.J.; Fang, M.; Liu, Y.W. Optimizing design of a new ZBO cryogenic storage tank in microgravity. *Energy Procedia* **2014**, *61*, 1942–1946.
10. Zhang, M.; Tang, W.X.; Wang, F.; Zhang, J.; Cui, W.C.; Chen, Y. Buckling of bi-segment spherical shells under hydrostatic external pressure. *Thin-Walled Struct.* **2017**, *120*, 1–8.
11. Rastgar, M.; Showkati, H. Buckling of cylindrical steel tanks with oblique body imperfection under uniform external pressure. *ASME J. Press. Vessel Technol.* **2017**, *139*, 203–213.
12. Azzuni, E.; Guzey, S. Stability of open top cylindrical steel storage tanks: Design of top wind girder. *ASME J. Press. Vessel Technol.* **2017**, *139*, 312–322.
13. Vathi, M.; Karamanos, S.A.; Kapogiannis, I.A.; Spiliopoulos, K.V. Performance criteria for liquid storage tanks and piping systems subjected to seismic loading. *ASME J. Press. Vessel Technol.* **2017**, *139*, 801–812.
14. Sweedan, A.M.I.; Damatty, A.A.E. Simplified procedure for design of liquid-storage combined conical tanks. *Thin-Walled Struct.* **2009**, *47*, 750–759.
15. Musa, A.; Damatty, A. Capacity of liquid-filled steel conical tanks under vertical excitation. *Thin-Walled Struct.* **2016**, *103*, 199–210.

16. Bonanos, A.; Votyakov, E. Sensitivity analysis for thermocline thermal storage tank design. *Renew. Energy* **2016**, *99*, 764–771.
17. Erdemir, D.; Altuntop, N. Improved thermal stratification with obstacles placed inside the vertical mantled hot water tanks. *Appl. Therm. Eng.* **2016**, *100*, 20–29.
18. Ansary, A.M.E.; Damatty, A.A.E.; Nassef, A.O. A coupled finite element genetic algorithm for optimum design of stiffened liquid-filled steel conical tanks. *Thin-Walled Struct.* **2011**, *49*, 482–493.
19. Bu, F.; Qian, C.F. On the rational design of the top wind girder of large storage tanks. *Thin-Walled Struct*. **2016**, *99*, 91–96.
20. Minoglou, M.K.; Hatzigeorgiou, G.D.; Papagiannopoulos, G.A. Heuristic optimization of cylindrical thin-walled steel tanks under seismic loads. *Thin-Walled Struct.* **2013**, *64*, 50–59.
21. Fan, J.; Furbo, S. Thermal stratification in a hot water tank established by heat loss from the tank. *Sol. Energy* **2012**, *86*, 3460–3469.
22. Niloufari, A.; Showkati, H.; Maali, M.; Fatemi, S.M. Experimental investigation on the effect of geometric imperfections on the buckling and post-buckling behavior of steel tanks under hydrostatic pressure. *Thin-Walled Struct.* **2014**, *74*, 59–69.
23. Lin, L.X. Micro-propulsion System for Modern Small Satellites. *Spacecr. Eng*. **2010**, *19*, 13–20.
24. Peng, L.; Liu, L.; Long, T.; Guo, X.S.; Shi, R.H. Satellite thruster configuration design based on propellant consumption optimization. *J. Astronaut.* **2015**, *36*, 268–277.
25. Li, Q.; Lv, Q. Application of electric propulsion on communications satellite platform. *Space Int*. **2016**, *451*, 46–52.
26. Li, H. Study on Preparation and Properties of Micro Thruster. Master's Thesis, Anhui Polytechnic University, Wuhu, China, 2015.
27. Yang, K.J. Stress Analysis of Pressure Vessel with Elliptical Cross Section. Master's Thesis, Xi'an Shiyou University, Xi'an, China, 2015.
28. Liu, P.; Xu, P.; Han, S. Optimal design of pressure vessel using an improved genetic algorithm. *J. Zhejiang Univ.-Sci. A* **2008**, *9*, 1264–1269.
29. Tsitas, S.R.; Kingston, J. 6 U Cubesat commercial applications. *Aeronaut. J.* **2012**, *116*, 189–198.
30. Wang, Z. Structural Optimization Design of Micro Thruster Based on Piezoelectric Transformer. Master's Thesis, Anhui Polytechnic University, Wuhu, China, 2015.
31. Xu, W.P. Structure Optimization in 3D Printers. Ph.D. Thesis, University of Science and Technology of China, Hefei, China, 2016.
32. Zhang, X.J.; Tang, S.Y.; Zhao, H.Y.; Guo, S.Q.; Li, N.; Sun, B.B.; Chen, B.Q. Research status and key technologies of 3D printing. *J. Mater. Eng*. **2016**, *2*, 122–128.
33. Salmi, L.M. Medical Applications of Additive Manufacturing in Surgery and Dental Care. Ph.D. Thesis, Aalto University, Espoo, Finland, 2013.
34. Lore, T.; Frederik, V.; Tom, C. A study of the micro-structural evolution during selective laser melting of Ti-6Al-4V. *Acta Mater*. **2010**, *58*, 3303–3312.
35. Zheng, Z.; Wang, L.; Feng, Y.B. Research progress of 3D printing metal materials. *Shanghai Nonferr. Metal*. **2016**, *1*, 57–60.
36. Tan, L.B.; Yu, X.H. Application and prospect of 3D printing in metal forming. *J. Netshape Form. Eng.* **2015**, *6*, 58–64.
37. Li, Y. Study on the Process and Properties of Porous Metal Prepared by Laser Additive Manufacturing (3D Printing). Master's Thesis, Soochow University, Suzhou, China, 2015.
38. Salmi, M.; Huuki, J.; Ituarte, I.F. The ultrasonic burnishing of cobalt-chrome and stainless steel surface made by additive manufacturing. *Prog. Addit. Manuf.* **2017**, *2*, 31–41.
39. Jiang, J.J. Study on the Microstructure and Properties of Biomedical Ti-6Al-4V Produced by Selective Laser Melting. Ph.D. Thesis, Chongqing University, Chongqing, China, 2015.
40. Wang, Y.; Jiang, J.J.; Qiao, L.Y.; Hu, D. Study on biological corrosion and biocompatibility of TC4 alloy by Selective Laser Melting. *J. Chongqing Univ.* **2015**, *3*, 21–27.
41. Wei, Q.; Li, Y.C. Technology of ammonia flashing jet propulsion in BX-1 satellite. *Manned Spacefl.* **2012**, *1*, 86–91.
42. Xu, H.; Yao, W.; Zhao, Y.; Wang, N.; Du, B.X. A step by step method for optimizing satellite structure. *Spacecr. Eng.* **2017**, *4*, 22–28.

43. Cheng, L. Design and Optimization of a Mass Production Satellite Structure. Master's Thesis, University of Chinese Academy of Sciences, Beijing, China, 2016.